ADVANCED MATERIALS INTERFACES
www.advmatinterfaces.de

Surface Stability of Azobenzene-Based Thin Films in Aqueous Environment: Light-Controllable Underwater Blistering

*Biagio Audia, Chiara Fedele, Caterina M. Tone, Gabriella Cipparrone, and Arri Priimagi**

Azobenzene-based light-responsive thin films are emerging as appealing candidates for smart cell-culture substrates. Their attraction lies in the fact that they can be reversibly photo-patterned, providing a route for dynamically mimicking the remodeling of the extracellular matrix. However, since the cells need to be cultured in aqueous environment, a key parameter in the layout of any biological application is the stability of the surface underwater. In this work, the authors perform a detailed investigation on the surface stability of azobenzene-based thin films in water and in a biologically relevant aqueous medium in which surface blistering occurs, as a result of water–material interaction. The phenomenon arises due to film delamination, and it can be prevented by changing the underlying substrate, by an additional coating layer, or by photo-induced control over the film permeability. It is also shown that the blister orientation can be controlled with polarized light. Furthermore, a simple model based on osmotic pressure is proposed to explain the blister formation. These findings provide a comprehensive overview of the interaction between water and the photo-responsive film surface, pertinent for engineering biomaterials with enhanced dynamic control over the cell–material interface.

1. Introduction

Smart responsive materials, which undergo significant structural transformations in response to external stimuli, have been widely explored in the last two decades due to their vast potential in applications such as additive manufacturing, civil engineering, and biomedicine.[1–6] Among them, azobenzene-based materials, due to their unique photo-responsive features, have attracted great attention for the remote and flexible control of materials properties via light stimulation.[7,8] The light response is triggered by photoisomerization of the azobenzene units using UV or visible irradiation,[9] providing the basis for a variety of photonic applications such as energy storage,[10,11] holographic recording,[12–14] soft robotics,[15,16] dynamic control of surface topology in liquid crystalline elastomers[17] and nonlinear optics[18,19] where, in particular, photoinduced reorientation allows for all-optical poling.[20] As one striking example, by controlling the impinging light configuration, the photoinduced processes in azobenzene-containing thin films invoke material mass migration that leads to the formation of topographic surface patterns, a prominent example being surface-relief grating (SRG) formation upon irradiation with a light interference pattern.[21–24] SRGs show great promise as diffractive photonic elements,[25,26] biosensing substrates,[27] or as nano-/microfabrication templates.[28–30]

The micron-scale periodicity of SRGs renders them an excellent fit for biological systems, many of which are composed of cells that are extremely sensitive to mechanical and topographic features of the surrounding microenvironment.[31,32] Hence, there is a growing interest in the use of azobenzene-based materials as smart bio-interfaces for cell culture.[33–35] The native extracellular matrix (ECM) of soft tissue is composed of entangled fibrous proteins,[36,37] as reproduced also in many synthetic ECM products.[38] Furthermore, ECM is continuously remodeled by the cells in physiological and pathological conditions.[39] Sinusoidal SRGs and embossed pillars in azobenzene thin films have been used for mimicking the ECM texture and controlling cellular directional migration in single and multiple cells,[40–42] directing axonal extension,[43,44] and determining stem cell fate.[45]

The most exciting characteristic provided by azobenzene-based systems lies in the reversibility of the photoinduced processes. It is well known that SRGs recorded in thin films can be erased by heating the sample above the glass transition temperature (T_g).[46,47] SRGs can be also efficiently erased and re-inscribed optically by using single-beam irradiation[24,48,49] or

B. Audia, C. M. Tone, G. Cipparrone
Physics Department
University of Calabria
Ponte P. Bucci cubo 33B, Arcavacata di Rende (CS) 87036, Italy
C. Fedele, A. Priimagi
Smart Photonic Materials
Faculty of Engineering and Natural Sciences
Tampere University
Korkeakoulunkatu 3, Tampere 33720, Finland
E-mail: arri.priimagi@tuni.fi
C. M. Tone
CNR-Nanotec c/o Physics Department
University of Calabria
Ponte P.Bucci cubo 33B, Arcavacata di Rende (CS) 87036, Italy
The ORCID identification number(s) for the author(s) of this article can be found under https://doi.org/10.1002/admi.202102125.

DOI: 10.1002/admi.202102125

spatially shifting the recording interference pattern.[24,50] Light-induced erasure, unlike the thermal one, acts locally and is non-damaging for cells, which must be cultured at 37 °C. In principle, switching "on-off" topographical features via light stimulation offers the possibility to dynamically control cell behavior,[51,52] opening up a wide range of in vitro bio-applications where the azobenzene-based materials mimic the ECM remodeling during different biological processes.[53]

Another important aspect in virtually any biological application is the ever-present aqueous environment (buffer solution, culture medium, etc.) that may affect the stability of the material surface, especially during the SRG formation and erasure. For instance, Rocha et al.[35] observed in a family of azo-polysiloxane thin films that long exposure to water leads to the formation of micrometer-sized structures (depending on the specific chemical composition of the material), which influences cell adhesion onto the film surface. Additionally, as reported by Rianna et al., the presence of an aqueous environment also affects the cellular response during the photo-erasure of the surface topography.[41] The authors observed that NIH-3T3 fibroblasts seeded on a Poly (Disperse Red 1—methacrylate) thin film and aligned along the sinusoidal SRGs, drastically changed their orientation due to the presence of bubble-like structures that arose on the film surface during underwater erasure of the microtopographic features. In both works, the undesired surface structures appeared due to the presence of the aqueous medium. To the best of our knowledge, no detailed explanation of the formation mechanism of these structures has been proposed. Such information would be extremely relevant for engineering biomaterials with enhanced dynamic control over the cell–material interface for more sophisticated investigations in cell biology.

Herein, we tackle the abovementioned phenomenon that takes place on the surface of an azobenzene-containing amorphous thin film. We coin the phenomenon water-induced blistering, and study it with a combination of experimental techniques. By means of digital holographic microscopy (DHM) and atomic force microscopy (AFM), we investigate in detail the film stability and its photo-responsive behavior in aqueous environment. We demonstrate that the formation of blisters is due to local delamination of the film from the substrate, triggered by water permeation toward the support underneath. Furthermore, we show that the choice of the substrate or the presence of a covering thin layer prevent the occurrence of the phenomenon. We also propose a simple blister formation mechanism based on the osmotic pressure model proposed by Berkelaar et al.[54] Finally, we show a light-aided way of controlling the blistering onset in aqueous environment and the reversible photocontrol over blisters orientation and shape.

2. Results

2.1. Underwater Surface Stability of the Azobenzene-Based Films

The morphological stability of the azobenzene-based thin film surface was tested in aqueous environment using Milli-Q water and in a biologically relevant aqueous medium such as Dulbecco's Modified Eagle Medium (DMEM). As material of choice for the present study we selected the Disperse Red 1 molecular glass (DR1-glass) introduced by Lebel et al.,[55] which we have already used as smart light-responsive cell support layer.[40,43] First, we inscribed SRGs onto the DR1-glass thin film and investigated the evolution of the surface in contact with Milli-Q water by combining DHM and AFM observations. These techniques provide quantitative information about surface morphology in a complementary fashion. DHM allows fast acquisition (down to 1 ms) of large-area topography, whereas AFM, even if slower (approximately minutes), enables local investigation with high lateral resolution.

A DHM quantitative phase image of the DR1-glass film surface after the SRG inscription is shown in **Figure 1**a. It presents a characteristic sinusoidal profile with the expected spatial periodicity (1 μm) and a relief depth of about 120 nm. The same area observed 60 min after adding a Milli-Q water droplet on the sample showed that the sinusoidal surface pattern had turned into a bumpy surface with large features whose height ranged from hundreds of nanometers up to 1 μm (Figure 1b). These objects, which appear all over the wet surface, are blisters that develop at the glass/DR1-glass interface and locally bulge the film that detaches from the substrate. Image analysis of Figure 1b shows that the distribution of the blisters' diameter (evaluated as Feret diameter, Figure 1c) ranges from few microns up to 16 μm, and that they are mostly circular in shape (Figure 1c,d). The typical blisters' surface profile, reported in Figure 1e, shows periodic ridges reminiscent of the SRG (Figure 1a), indicating that the blisters arise as a result of local detachment of the film from the substrate.

The water-induced blistering phenomenon is not directly related to the presence of the SRG. As reported in Figure S1, Supporting Information, AFM topographic acquisition performed on a flat DR1-glass thin film before and 60 min after adding Milli-Q water into the sample chamber revealed a surface evolution comparable to the one reported in Figure 1b. In order to understand the processes that lead to the blister formation, we performed a time lapse imaging with both DHM and AFM on a flat area of the DR1-glass film surface in contact with water. The series of DHM intensity images shown in **Figure 2** highlights the characteristic phases we identified in the blisters' formation dynamics: nucleation, coalescence, and growth. In some cases, their formation seems to be localized around topographical defects (TDs), that is, small material aggregates or "impurities" (Figure 2a), which act as nucleation points pinning the blister position. Once formed, the blisters tend to coalesce into larger structures (see Figure 2b,c) and then grow in height without changing their lateral size (Figure 2d,e). The experiment was performed using previously degassed Milli-Q water. Tests carried out with non-degassed water produced similar results, confirming the nature of the phenomenon as water-induced blistering as opposed to the formation of gaseous domains as happens for microbubbles.[56] The dynamics of blister formation was influenced by the film wettability, material type, and thickness (see Figure S2–S4, Supporting Information).

We also followed the evolution of the film surface in contact with water using AFM (**Figure 3**). To ease the blisters detection, we selected for the analysis an area of the film where a TD was easily identifiable. Figure 3a shows the selected area before

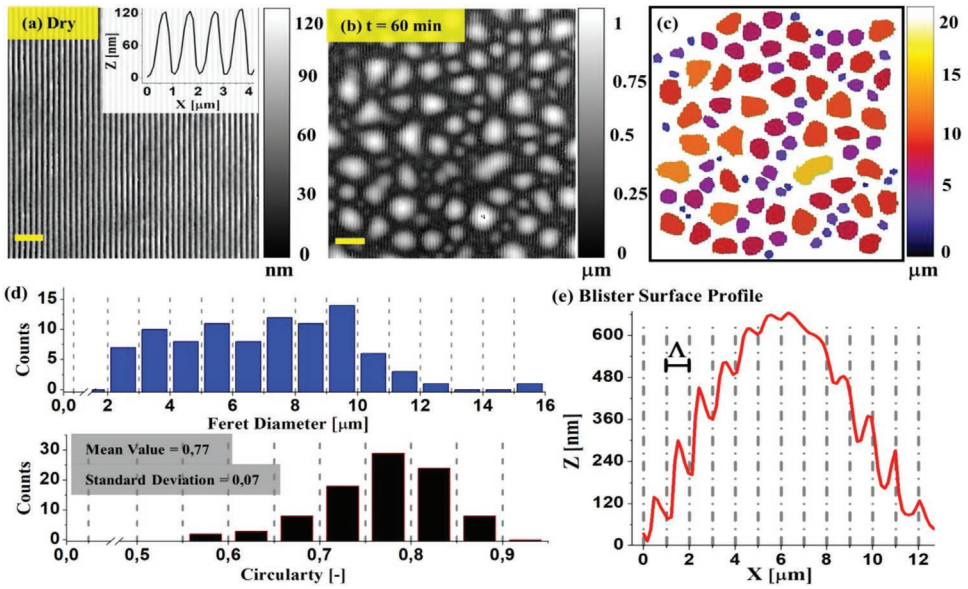

Figure 1. DHM quantitative phase image of the DR1-glass film surface a) immediately after the SRG recording and b) 60 min after adding a droplet of Milli-Q water on the sample; for both images, the *z*-scale is reported on the right, the scale bar is 5 µm in (a) and 10 µm in (b). The inset in (a) shows a representative SRG profile in dry environment. c) Color map of the blisters' Feret diameter obtained from the binarized image of (b); the color-scale is reported on the right. d) Distribution of the blisters' Feret diameter (top, blue histogram) and circularity (down, black histogram) evaluated over a population of 92 blisters; the grey dotted lines represent the bin size. e) Typical blisters' surface profile. The grey dotted lines represent the SRG periodicity.

adding Milli-Q water; Figure 3b shows the same area imaged 30 min after the addition of Milli-Q water onto the sample. Figure 3c presents an overlap of the TD and blisters outline profiles obtained from Figure 3a,b. Looking at the blister indicated as B2, it can be seen that the TD pinched its position and the blister developed on the TD's side. The presented AFM analysis not only supports the DHM observations on the blister formation dynamics, but also highlights the role of TDs in the process. We next studied the DR1-glass surface stability in DMEM. Also in this case, as shown in Figure S5, Supporting Information, we observed the surface blistering as consequence of the presence of the medium. The blisters were circular in shape and reached similar lateral dimensions to those reported in Milli-Q water.

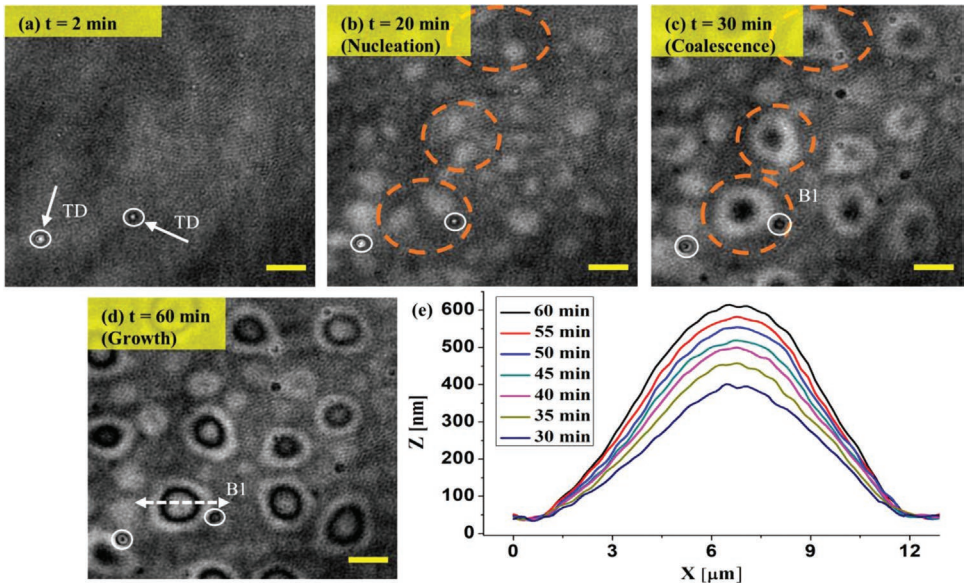

Figure 2. a–d) DHM intensity images representing the temporal evolution of the DR1-glass film surface in contact with previously degassed Milli-Q water; the scale bar is 10 µm. The white arrows and the white circles highlight the topographical defects (TDs) present at the interface which act as nucleation centers by pinning the blisters position. The dashed orange circles highlight the occurrence of coalescence. The dark and bright fringes are the result of the interference from the light reflection at the continuous curved surface of the blisters. e) Surface profile of the blister indicated as B1 acquired, from the respective quantitative phase images, at different times.

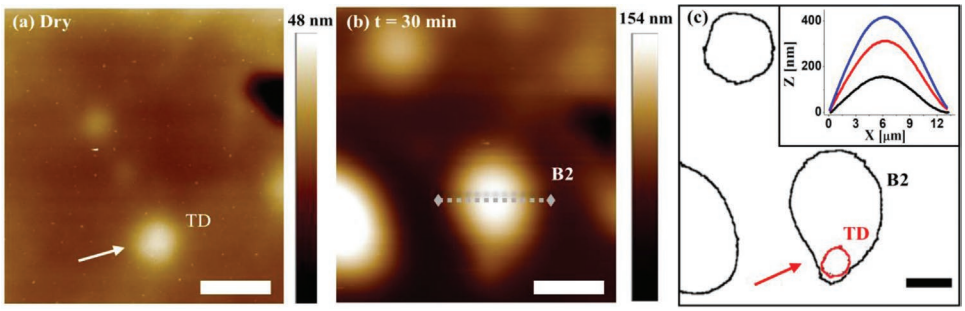

Figure 3. AFM topography images of DR1-glass surface in a) dry environment and b) 30 min after the addition of Milli-Q water onto the sample; the white arrow indicates the topographical defect (TD), the *z*-scales are reported on the right and the scale bar is 10 µm. c) TD (red line and red arrow) and blisters (black lines) outline profiles obtained from the binarized mask image of (a) and (b); the scale bar is 10 µm. The inset shows the surface profile of the blister B2 imaged along the grey dotted line in (b) at different times (30 min black line, 45 min red line, and 60 min blue line) after the addition of Milli-Q water.

While the previous analyses show that the blistering of the surface is induced by the presence of an aqueous environment, the removal of the latter induce a strong modification on the film morphology. As shown in Video S1, Supporting Information, about 2 min after water removal the blisters were not visible anymore in the DHM images. More insight on the blister's evolution after medium removal, was gained through AFM analysis (**Figure 4**), which show that the blisters collapsed. The blister shown in Figure 4a, which in water had reached a height of about 750 nm, resulted in a crater of the same lateral dimension after medium removal, indicating deflation of the structure (Figure 4b,c). An image acquired over a larger area is shown in Figure 4d and provides an overview of the dried film surface. The same behavior has been found also after the removal of the DMEM (Figure S5, Supporting Information).

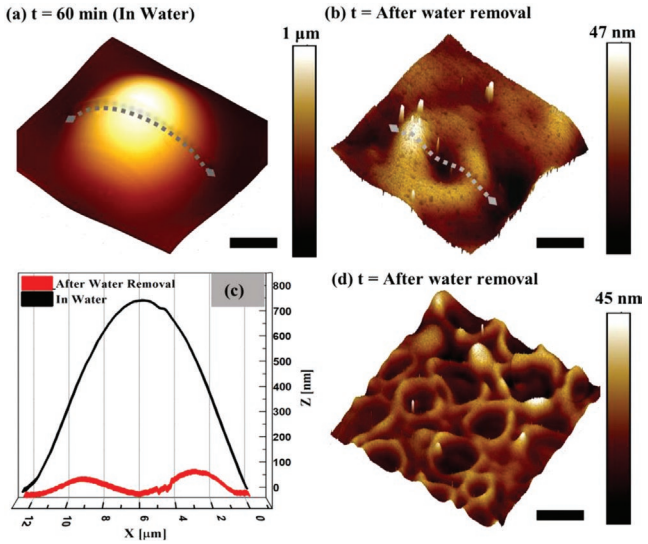

Figure 4. 2.5 D AFM surface topography reconstruction of a single blister area a) before and b) after the Milli-Q water removal from the DR1-glass film; the z-scales are reported on the right, the scale bar is 2 µm. c) The grey dotted lines represent the surface profiles shown in graph (black line: in water, (a); red line: after water removal, (b)). d) Overview of the dry film topography after the water removal; the *z*-scale is reported on the right, the scale bar is 10 µm.

2.2. Photo-Control over Blister Shape and Formation

Azobenzene-containing materials respond to light in many ways.[57] Single azobenzene molecules tend to progressively orient perpendicularly to the polarization direction,[58] driving the macroscopic material migration and the formation of the topographical patterns.[59,60] Microstructured azobenzene materials, such as microparticles and pillars, are able to deform in response to polarized light, elongating in the polarization direction.[61,62] Therefore, we hypothesized that the blister formation could also be photo-controlled.

As first test we investigated the underwater photo-responsive behavior of the blistered DR1-glass film surface with SRG, shown in Figure 1. After 60 min in Milli-Q water (Figure 1b) the area was irradiated for 300 s with horizontally polarized (P) continuous-wave laser source (488 nm, 10 mW mm^{-2}) coupled to DHM. The dynamics of the process was followed with DHM, and already from the first seconds of irradiation, reshaping of the blisters occurred. A comparison between the blistered surface before (**Figure 5**a) and after (Figure 5b) exposure shows how the blisters deviate from their initial almost circular shape to an elliptical shape oriented along the polarization direction. As shown in Figure 5c, parallel to the deformation, a good degree of photo-erasure of the SRG is also obtained: the amplitude of the grating was reduced by 80% from ≈100 to ≈20 nm, demonstrating that the presence of water does not seem to limit the optical erasure. In Figure 5d, quantitative analysis of the deformation is performed by fitting the shape of the blisters with an ellipse (red outlines in Figure 5a,b) and evaluating at different times the roundness R of the objects. During the exposure $\langle R \rangle$ varies from its initial value of 0.85 ± 0.09 to 0.51 ± 0.1, confirming the observed light-induced reshaping. In addition to reconfiguring the shape of the blisters, irradiation also stabilizes them on the surface, providing a water-assisted route to photo-pattern the azobenzene films. Figure 5e reports the optical microscope (OM) image of the exposed area after the medium removal and leaving the sample overnight in the oven at 60 °C in order to achieve complete water evaporation.

Within the irradiated area the blisters remain fixed on the surface, preserving the photo-induced orientation and the elliptical shape, instead of collapsing upon water removal, as could be expected based on the Video S1, Supporting Information

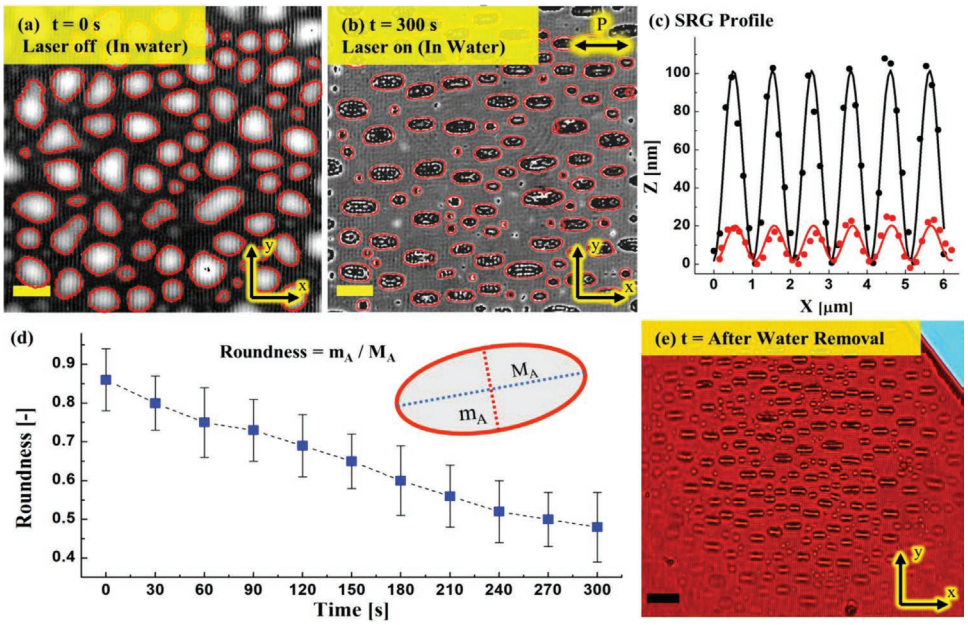

Figure 5. DHM intensity images of the blistered DR1-glass SRG in Milli-Q water a) before and b) after 300 s irradiation with horizontally polarized (P) laser beam; the scale bar is 10 μm. c) Representative SRG profile before (black dots) and after (red dots) irradiation; the profiles are superimposed with a sine function (black and red lines) to better highlight the photo-erasure process. d) Roundness versus irradiation time, evaluated over a population of 58 blisters (blue squares: mean values, error bar: standard deviation). The statistical analysis has been performed including only the blisters observable before the irradiation. e) Optical microscope bright field image of the irradiated area after the Milli-Q water removal; the scale bar is 20 μm.

and Figure 4 (no light irradiation). By changing the polarization of the incident laser to vertical (the direction along the grating grooves), the blisters align accordingly, while the dynamics of the blister photo-elongation remains unchanged (Figure S6a,b, Supporting Information). Also in this case, the blisters are stabilized on the film surface (Figure S6c, Supporting Information) and SRG photo-erasure takes place with an amplitude decrease of around 85% (Figure S6d, Supporting Information).

Furthermore, as displayed in **Figure 6**, the underwater photo-control over the blister's orientation was reversible. The figure reports the analysis of the images acquired by DHM in a blistered area of the sample before (Figure 6a) and after two consecutive laser irradiations with orthogonally polarized laser beams (Figure 6b,c, 488 nm, 40 s, 10 mW mm^{-2}).

It can be seen how blisters already oriented along the vertical axis ($<\theta> = 91 \pm 4°$) following the first exposure to vertical polarization, changed their orientation along the horizontal one ($<\theta> = 5 \pm 3°$) upon second exposure with orthogonal polarization. The manual 90° switch between the two polarization states provokes a corresponding variation of the blister's orientation ($\Delta\theta \approx 86°$), while the aspect ratio (AR) and the roundness (R) of the ellipsoidal objects remain practically unchanged, suggesting that the re-orientation occurs simply through rotation of the blisters in the *xy*-plane. However, we also observed that, as the blister size increases, this re-orientation effect may involve the separation of bigger blisters into smaller ones.

We also studied the underwater irradiation of the SRG with blisters using a LED. As reported in Figure S7, Supporting Information, also LED exposure induces reshaping of the

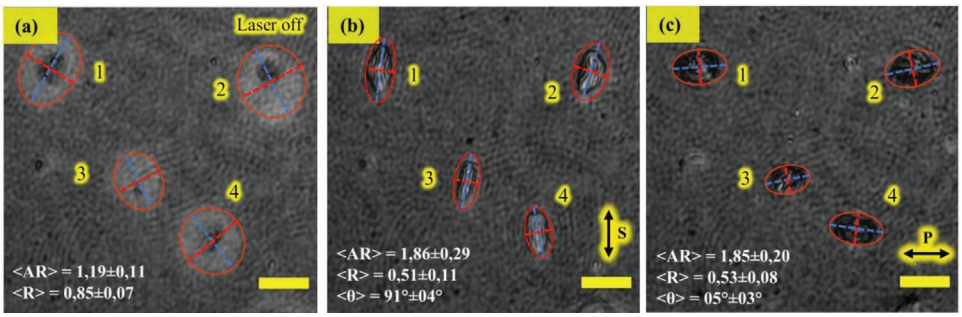

Figure 6. DHM intensity images acquired, in Milli-Q water, on a blistered area of the DR1-glass film surface a) before and b) after two consecutive 40 s irradiation with laser beam linearly polarized first along the vertical axis and c) after along the horizontal axis. For each image the scale bar is 10 μm. The red lines represent the outline profiles of the blisters obtained fitting their shape with an ellipse, whereas the dotted lines are the major and minor axes of such ellipses. In the text boxes the average values of aspect ratio (AR), roundness (R), and orientation (θ) of the ellipsoidal objects recognized by the software are reported.

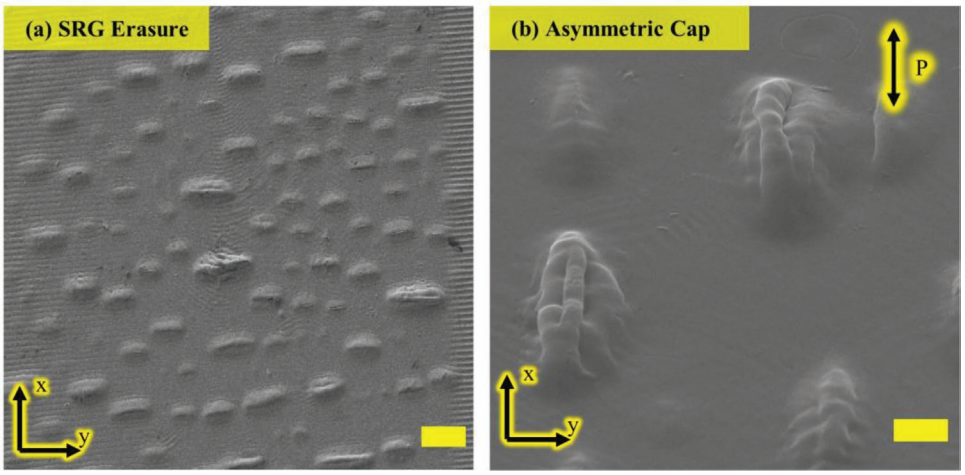

Figure 7. SEM images, after the Milli-Q water removal, of the blistered SRG areas irradiated with laser light. a) Image of an entire irradiated area (vertical polarization) which clearly highlights the SRG photo-erasure and the blisters orientation. b) Detail of the blister morphology after the irradiation (horizontal polarization) which evidence the asymmetric cap. For both images the scale bar is 10 µm.

blisters (which orient along its main polarization direction), their stabilization on the film surface, and a degree of grating erasure comparable with the results obtained for laser light (Figures 5c,6d). In **Figure 7**, scanning electron microscopy (SEM) images of the different irradiated zones are reported after the removal of the aqueous medium and leaving the samples overnight in the oven at 60°. The high spatial resolution offered by the instrument provides further details regarding the blisters' morphology after stabilization with light. Typical SEM images of the blistered surface after exposure to linearly polarized laser light are shown in Figure 7b. It can be noted how the photo-induced deformation acted not only on the bearing structure of the blisters, orienting it along the polarization direction, but even on the upper part, giving rise to an asymmetric cap oriented along the same axis. Similar asymmetric photo-deformation was observed also after the LED irradiation (Figure S7e, Supporting Information).

Blisters stabilization and orientation are not the only means of controlling the surface topography provided by light. Through irradiation, it was possible to directly modify the interfacial properties of the film, avoiding the blister formation. We followed the evolution of the film surface in contact with Milli-Q water observing a region of the sample that, immediately after the addition of liquid, was exposed to LED (4 mW mm^{-2}, 1 min). **Figure 8**a shows the boundary of this initially irradiated area after 60 min. It can be seen that the blisters developed only outside the light-treated zone, while in the irradiated area a different pattern, featuring smaller bumps (0.3–0.7 µm width), was formed. This additional pattern is formed during the initial irradiation phase and does not undergo any further morphological change during the remaining observation time. Following water removal, the developed blisters outside the exposed zone collapsed (Video S1, Supporting Information), while the smaller bump pattern remained stably on the film surface and clearly observable with OM (Figure 8b). The AFM topography of the initially irradiated area, shown in Figure 8c, revealed an inhomogeneous structuration of the film surface. The peaks of the height pattern, characterized by a cylindrical shape with a

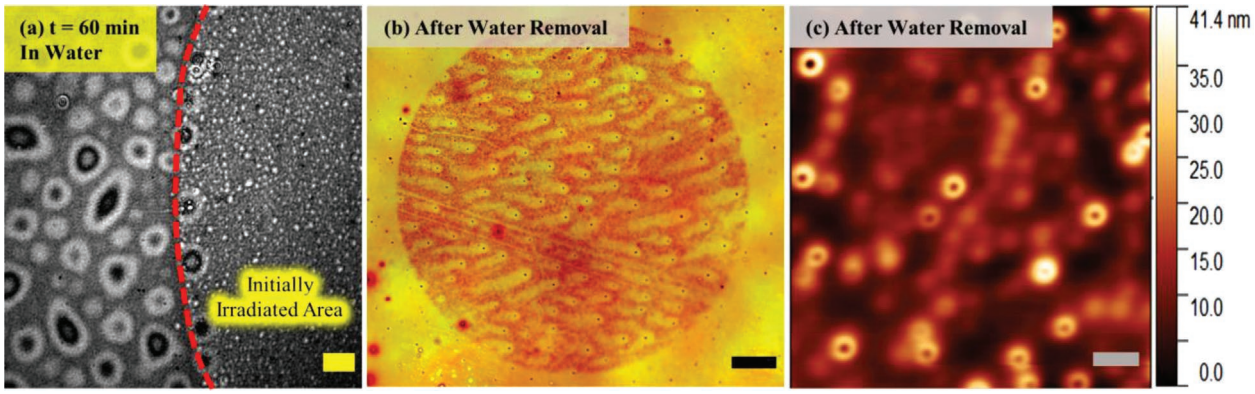

Figure 8. a) DHM intensity image of DR1-glass film surface 60 min after Milli-Q water addition. The image shows the boundary between the initially irradiated area (right side) and the adjacent unexposed zone (left side); the scale bar is 10 µm. b) Optical microscopy images of the entire irradiated area after water removal; the scale bar is 50 µm. c) AFM topography image of the irradiated area after the water removal; the *z*-scale is reported on the right, the scale bar is 1 µm.

height of about 30 nm, constitute distinct micro-domains well delineated from valleys.

However, the presence of water resulted a necessary condition for this pattern to occur, as it did not form when the same irradiation was performed in dry environment. The experiment was repeated using the laser source instead of LED, producing a similar pattern (Figure S8, Supporting Information).

3. Discussion

3.1. Blister Formation

The interactions at the interface between water and the material's surface have been widely investigated. Over the past decade, particular attention has been devoted to the study of thin films of polystyrene (PS) that, owing to the relative ease in the preparation and to the well-documented material properties, provide a good reference for studying such interactions. As a result of the contact between water and PS films, different surface phenomena such as nano-/microbubbles formation[63–66] and dewetting[67–71] have been reported and discussed by several research groups. Water-induced surface blistering is also included in the family of these phenomena and, despite the different chemical structure between PS and DR1-glass, several articles reported experimental results similar to those observed herein, both in terms of dimensions reached by the blisters and of the time scale in which they form (Figure S3, Supporting Information).[54,72–74] In addition, different theoretical models and mechanisms of formation have been suggested to explain the surface blistering.[54,75–77] Among them, the quantitative model proposed by Berkelaar et al.[54] based on the onset of an osmotic pressure gradient, well fits our experimental results. The authors ascribe the blister growth to delamination of the film from the substrate due to an osmotic flow of water beneath the film. They also observed a similar formation dynamics characterized by nucleation and growth, topological defects acting as nucleation sites, coalescence of blisters, and their deflation upon water removal.

We propose a simple mechanism for blisters formation, sketched in **Figure 9**, centered on the experimental results shown in Section 2.1 and based on the osmotic pressure model introduced above. As an initial step, water, which is a non-solvent for the DR1-glass, comes to contact with the film surface and starts permeating through the hydrophobic thin film toward the substrate.

Permeation could be driven by a higher affinity of water to the hydrophilic glass substrate (Figure S9, Supporting Information). Once permeated, water condenses around the TDs. Here, solute particles present at the glass interface begin to diffuse into the water pockets, increasing the osmotic pressure. The ensuing pressure gradient forces an increasing amount of water to flow through the DR1-glass toward the underneath support (Figure 9a). These solutes could be contaminants present in the DR1-glass and/or impurities at the glass–film interface. For instance, it has been shown that trace amount of solvent can remain stuck in polymer films and at the substrate interface after spin-coating.[78–81]

In response to the water flow, the film starts to bulge, triggering the growth step of the blisters. Once the osmotic pressure

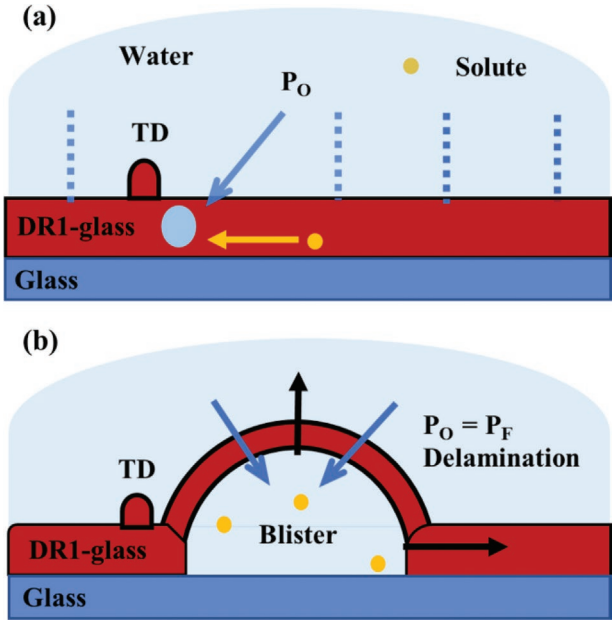

Figure 9. Sketch of the proposed mechanism for the blisters' formation. a) Penetration of water through the DR1-glass film surface, nucleation around the TD, and osmotic flow of water through the film driven by the osmotic pressure gradient. b) The blister's growth is allowed by the delamination of the film from the substrate. This condition occurs at the equilibrium between osmotic pressure and fracture pressure.

inside the blisters (P_O) equalizes the fracture pressure (P_F), which is the minimum pressure needed for the delamination of the film to occur,[77] the blister starts to grow radially and in amplitude (Figure 9b). During this phase, the film is stretched and probably plastically deformed, causing the blisters to coalesce (Figure 2c), and eventually to collapse (Figure 4) upon water removal.

The delamination mechanism might account for the key role that TDs seem to play in the blister formation process. To allow propagation of the delamination, the film has to crack at the edges of the blister.[77] Based on Griffiths' theory, the critical stress needed to propagate the delamination is inversely proportional to the crack length at the interface between the layers.[82] The presence of TDs might cause a critical increase in the crack length, translating into a lower critical stress, and thus allowing the growth of the blisters, pinched by topological defects (Figures 2,3c).

3.2. Photo-Controlled Blister Shape and Formation

The light-induced deformation of the blisters reported in Section 2.2 resembles in many aspects the deformation dynamics of azobenzene-containing soft matter, for example, azobenzene-containing microspheres and micropillars.[62,83–87]

Also in those cases, an elongation of the particles and pillars in the light polarization direction occurs, leading to the formation of highly anisotropic and asymmetric structures. The deformation of bulk microspheres, for instance, has been studied both in air and water, and differences in the deformation were observed.[61,88] In particular, the higher the refractive

index of the immersion medium, the more prominent the mass transport parallel to the substrate. Furthermore, in bulk microspheres and pillars the deformation took place only at the top surface due to the high absorbance of the material and the consequent rapid light attenuation inside the particle, leading to mushroom-shaped structures.[89] As reported by Loebner et al., light-induced deformation of azopolymer microspheres generated forces as high as 37 MPa when embedded in an elastomeric medium.[83] These observations may help explaining the results reported herein even further. In our case, the blisters may act as "microparticles," whose aspect ratio increases in the light polarization direction. However, our "particles," that is, the blisters, are not bulk and therefore they deform throughout the whole blister and not only on the upper surface. Studies on hollow microspheres have also shown the formation of tapered ends after long (≈30 min) light exposure times.[90] The results proposed in this work could open a new path for the development of reconfigurable water-assisted techniques for surface photo-patterning (Figure 6).

The reported observations show also how an initial underwater irradiation phase of the film surface (when the blisters were not developed yet) prevents the formation of blisters (which developed only outside the initially irradiated area) due to the formation of an additional pattern characterized by smaller features (Figure 8). The spontaneous formation of small periodic surface structures upon irradiation with a uniform light beam has been observed by different research groups, but a universal explanation of such intriguing effect has not been agreed upon yet.[91–94] It is thought to be associated with interference phenomena resulting from the interaction between the primary irradiation beam and secondary waves arising from the surface or related to scattering by surface defects. Besides the mechanistic aspects of this process, all the proposed theories are compatible with the observation of spontaneous periodic structures that optimize the diffraction of the irradiating beam and whose morphology and periodicity can be tuned by irradiation conditions and layer thickness.[91,95,96]

We also observed spontaneous formation of small features upon irradiation with LED or a single laser beam. In our working conditions, water is replacing air as the interfacial medium, and its presence plays a key role in the processes, since the film structuring was not observed in dry environment. Furthermore, this sub-micrometer pattern was not observed during the "normal" blister growth (aqueous environment, Figure 2), suggesting that the phenomenon is due to a coupled light-water effect in the beginning of the process. We may speculate that the rise of the spontaneous pattern might be connected to a photo-induced phase separation between the azobenzene isomers (*cis* and *trans*), similarly to what was reported by Galinski et al.,[95] promoted here by the aqueous environment. In this work the authors proposed a theoretical model to describe how the phase separation alters the local evolution of the two isomers' concentration, which is directly connected to the material surface structuration through the different physical and chemical characteristics of the two isomers. After light irradiation, a film topography resembling that reported in Figure 8c was observed, characterized by cylindrical peaks and valleys. Within our experimental framework, the presence of water, which is readily penetrating beneath the glassy thin film, could promote the photo-induced phase separation, and the consequent spontaneous surface pattern formation, shifting the *cis*/*trans* equilibrium toward the *cis* isomer.[97] This photo-induced structural change in the material, may reflect on the permeability properties of the film, as already reported in the case of gas permeation,[98,99] blocking the subsequent establishment of the water osmotic flow and thus preventing the blisters growth. A similar kind of result was obtained by Huang et al.[100] where a dynamic control over on/off porosity, in layer-by-layer azobenzene-based thin films was achieved combing light irradiation and water environment. The findings discussed above, although they certainly need additional study, outline DR1-glass as a promising candidate for the development of new light-responsive membrane.[101]

3.3. Blisters Prevention

On the one hand, the water-induced blistering of azobenzene-based thin films represents a fascinating phenomenon worthy of further investigation and of potential utility. On the other hand, for specific applications, the occurrence of blistering may be an undesired effect and hence it is worth to investigate how to prevent it.

A simple route to prevent surface blistering is evident by the proposed osmotic model (Section 3.1). Since the first step of the mechanism requires a higher affinity of water toward the hydrophilic substrate than the hydrophobic film surface to trigger water permeation, we followed the surface evolution in aqueous environment while modifying the underneath glass hydrophilicity by a 12 nm-thick gold-sputtered layer (Figure S9, Supporting Information). In this case, as reported in Figure S10a,b, Supporting Information, the formation of blisters was completely prevented. Similar results were obtained also for DMEM (Figure S10c,d, Supporting Information). These observations, in addition to providing a simple way to prevent surface blistering underwater, contextually confirm the applicability of the model to the obtained experimental results. Another simple way to avoid the blisters formation, as shown in Figure S10e,f, Supporting Information, is to cover the DR1-glass film with a thin layer of polydimethylsiloxane (PDMS; ≈60 nm). The latter acts as an additional "barrier," retarding contact between water and the material's surface and changing the conditions at the interface. PDMS is widely used in many biological applications.[102] Therefore, an additional advantage of this blistering prevention approach lays in its compatibility with well-known protein deposition techniques. Furthermore, PDMS coating does not impair SRG formation and erasure, reducing the blisters formation upon light irradiation.[103]

4. Conclusions

The stability of a material surface underwater is a crucial parameter especially in applications related to cell culture, which necessarily requires the presence of an aqueous environment. In this work we tested the surface stability and the photo-responsive behavior of an azobenzene-based thin film in Milli-Q water and in a biologically relevant water-based medium,

DMEM. As principal result of the interaction with the aqueous environment, surface blistering occurred. Such blisters were almost circular in shape, reaching heights from hundreds of nanometers up to 1.5 μm, and characterized by a lateral size in the range 1–15 μm. This local film bulging originates from the film delamination from the substrate because of an osmotic flow that leads to water permeation through the surface toward the hydrophilic glass support. We demonstrate that the stability of the material surface can be easily preserved, avoiding blistering, by using a more hydrophobic substrate or covering the film with a thin layer of PDMS.

The results described in this study can also be interpreted from a different perspective. The surface blistering process could be exploited as a new water-assisted photo-patterning technique of azobenzene-based thin films. By irradiation with a suitable wavelength, it is possible to stabilize such structures on the material surface and additionally change their orientation and shape according with light polarization. Moreover, light irradiation enables control over the blister formation by directly acting on the film interface properties, changing its water permeability.

We are confident that our findings are relevant for microfabrication of light-responsive materials with enhanced dynamic control over the cell–material interface and may inspire future more sophisticated investigations in cell biology.

5. Experimental Section

Preparation of Photosensitive Thin Films and SRG Inscription: The azobenzene-containing glass-forming material (Disperse Red 1 molecular glass, DR1-glass, Solaris Chem Inc., Figure S11a, Supporting Information) was dissolved in chloroform (7% w/v) and filtered through a nylon filter with 0.45 μm pore size (Corning Incorporated). The solution was dispensed over two different substrates (conventional microscope glass slide and gold-deposited slide) by spin coating (Laurell Technologies Corporation) at 1500 rpm for 30 s, yielding uniform, high-quality thin films with thickness of 490 ± 10 nm measured by a Veeco Dektak-8 profilometer. The microscope slides (Thermo Fisher) were washed with distilled water and isopropanol and then ultrasonicated twice in acetone for 10 min. The gold layer was deposited at room temperature by DC Sputtering on a precleaned glass substrate using a Vacuum Lab Coater (HHV Auto 306). The resulting thickness was measured by using an ellipsometer (M2000 Woolam) and it turned out to be ≈12 nm. PDMS covering layer was obtained by dissolving a 1 wt% solution of PDMS precursors (1:10 ratio) in n-hexane, followed by spin coating onto DR1-glass films at 6000 rpm for 2 min 30 s. The film was then cured in the oven at 60 °C for 2 h.

The SRGs were inscribed using a Lloyd's mirror interferometer.[21] The inscription was performed with a 488 nm continuous-wave laser (Coherent Genesis CX488-2000), irradiating the sample for 10 min with an intensity of 300 mW cm^{-2} over an area of 0.25 cm^2. To ensure efficient SRG formation, a circularly polarized recording beam was used.[104] The grating period Λ is given by $\Lambda = \lambda/2\sin\vartheta$, where λ is the laser wavelength and ϑ is the angle between the laser beam and the sample normal. The interferometer set-up was set to obtain $\Lambda = 1$ μm.

Digital Holographic Microscopy: Digital holographic microscope (DHM R-2100, Lyncèe tec.) was used as a quantitative phase imaging technique to monitor the surface evolution and the photo-responsive behavior of the DR1-glass thin films underwater (≈1 mL droplet size). By measuring both the amplitude and the phase of the light reflected from the sample, DHM quantitatively reconstructed the surface modulation from the sample hologram.[105] The microscope was equipped with a 40× water-immersion objective (0.8 NA, Olympus LUMPLFLN40XW). The instrument was coupled to a 488 nm optically pumped semiconductor laser (Coherent Genesis CX-488 2000) via a one-to-two beam-splitting, polarization-maintaining, single-mode optical fiber (Thorlabs PN480R5F1). Furthermore, a 470 nm LED source (Thorlabs M470L3 Mounted LED) was coupled to the instrument via a fiber patch cable (Thorlabs M28L01). Both wavelengths of the used external sources fall into the absorption band of the DR1-glass (Figure S11b, Supporting Information).

Atomic Force Microscopy: The topographic images of DR1-glass thin films were acquired using the Bruker Multimode 8 AFM equipped with a Nanoscope V controller. The measurements were carried out at room temperature, in tapping mode, using silicon cantilevers (model TAP150, Burker). To study and monitor the blister formation in the fluid environment, the Fluid Cell-MMTMEC Bruker device was used. Topographic images of the same region of the sample at different times, as well as after drying, were acquired. Milli-Q water (Millipore Corporation), and DMEM (Sigma Aldrich) were used as fluid media. For each image acquired using the fluid cell a volume of ≈20 μL was utilized. All the topographic images were analyzed using the Nanoscope Analysis software (Bruker) and the WSxM software.[106] The image reported in Figure 8 was taken with a Park XE-100 AFM (Park Systems) in non-contact mode in air with an Al-coated Si ACTA probe (AppNano) with 200–400 kHz nominal frequency and 13–77 N m^{-1} spring constant.

Scanning Electron Microscopy: The SEM imaging was performed with a focused ion beam SEM (Zeiss Crossbeam 540, Carl Zeiss AG). Images were taken both in top and tilted view (36°). Before SEM analysis, the samples were sputter-coated with a thin layer of silver.

Optical Microscopy: Bright-field imaging was performed with the OM Zeiss Axio Scope A1 (Carl Zeiss AG).

Image Analysis: The image analysis was performed using ImageJ software[107] with the "Analyze Particles" plugin. Before performing a pattern recognition, the raw images acquired with DHM were thresholded and binarized. As a result, a set of generally elliptical individual objects was recognized from each image. An array of geometrical parameters including: Feret diameter, area, perimeter, major axis, minor axis, orientation, and circularity ($4\pi \times$ area/perimeter^2) were extracted for all individual objects in the images and used for further analysis. Mean values and standard deviation were calculated in order to analyze the statistical significance of the geometrical parameters involving a large population of blisters.

Supporting Information

Supporting Information is available from the Wiley Online Library or from the author.

Acknowledgements

B.A. acknowledges POR Calabria FESR/FSE 2014–2020 for financial support. C.F. is thankful to the Finnish Cultural Foundation for the financial support. C.M.T. acknowledges PON "Attraction and International Mobility" R&I 2014–2020, AIM 1875705-2, CUP H24119000450005, for financial support. Dr. Turkka Salminen and the Tampere Microscopy Centre are acknowledged for performing SEM imaging. The authors also want to acknowledge the Academy of Finland Flagship Programme, Photonics Research and Innovation (PREIN, Decision number 320165) and the Emil Aaltonen Foundation.

Conflict of Interest

The authors declare no conflict of interest.

Data Availability Statement

The data that support the findings of this study are available from the corresponding author upon reasonable request.

Keywords

azobenzene, surface blistering, surface patterning, photo-responsive materials

Received: October 30, 2021
Revised: December 13, 2021
Published online: February 2, 2022

[1] S. Bahl, H. Nagar, I. Singh, S. Sehgal, *Mater. Today: Proc.* **2020**, *28*, 1302.
[2] K. R. Ryan, M. P. Down, C. E. Banks, *Chem. Eng. J.* **2021**, *403*, 126162.
[3] R. Huang, S. Zheng, Z. Liu, T. Y. Ng, *Int. J. Appl. Mech.* **2020**, *12*, 2050014.
[4] Z. Zhang, K. G. Demir, G. X. Gu, *Int. J. Smart Nano Mater.* **2019**, *10*, 205.
[5] V. Cardoso, D. Correia, C. Ribeiro, M. Fernandes, S. Lanceros-Méndez, *Polymers* **2018**, *10*, 161.
[6] S. Jerzy, *IOP Conf. Ser.: Mater. Sci. Eng.* **2020**, *958*, 012006.
[7] *Smart Light-Responsive Materials* (Eds: Y. Zhao, T. Ikeda), John Wiley & Sons, Inc., Hoboken **2009**.
[8] E. Merino, M. Ribagorda, *Beilstein J. Org. Chem.* **2012**, *8*, 1071.
[9] H. M. D. Bandara, S. C. Burdette, *Chem. Soc. Rev.* **2012**, *41*, 1809.
[10] S. Li, H. Wang, J. Fang, Q. Liu, J. Wang, S. Guo, *J. Therm. Sci.* **2020**, *29*, 280.
[11] Z. Wang, R. Losantos, D. Sampedro, M. Morikawa, K. Börjesson, N. Kimizuka, K. Moth-Poulsen, *J. Mater. Chem. A* **2019**, *7*, 15042.
[12] B. Audia, M. A. Bugakov, N. I. Boiko, P. Pagliusi, G. Cipparrone, V. P. Shibaev, *Macromol. Rapid Commun.* **2020**, *41*, 2000384.
[13] E. Zarins, K. Balodis, A. Ruduss, V. Kokars, A. Ozols, P. Augustovs, D. Saharovs, *Opt. Mater.* **2018**, *79*, 45.
[14] A. Shishido, *Polym. J.* **2010**, *42*, 525.
[15] M. Lahikainen, H. Zeng, A. Priimagi, *Nat. Commun.* **2018**, *9*, 4148.
[16] X. Pang, J. Lv, C. Zhu, L. Qin, Y. Yu, *Adv. Mater.* **2019**, *31*, 1904224.
[17] D. Liu, C. W. M. Bastiaansen, J. M. J. den Toonder, D. J. Broer, *Angew. Chem., Int. Ed.* **2012**, *51*, 892.
[18] S. K. Yesodha, C. K. Sadashiva Pillai, N. Tsutsumi, *Prog. Polym. Sci.* **2004**, *29*, 45.
[19] Q. Xie, Z. Shao, Y. Zhao, L. Yang, Q. Wu, W. Xu, K. Li, Y. Song, H. Hou, *Dyes Pigm.* **2019**, *170*, 107599.
[20] C. Fiorini, F. Charra, J.-M. Nunzi, P. Raimond, *J. Opt. Soc. Am. B* **1997**, *14*, 1984.
[21] P. Rochon, E. Batalla, A. Natansohn, *Appl. Phys. Lett.* **1995**, *66*, 136.
[22] P. Pagliusi, B. Audia, C. Provenzano, M. Piñol, L. Oriol, G. Cipparrone, *ACS Appl. Mater. Interfaces* **2019**, *11*, 34471.
[23] M. Salvatore, F. Borbone, S. L. Oscurato, *Adv. Mater. Interfaces* **2020**, *7*, 1902118.
[24] J. Jelken, S. Santer, *RSC Adv.* **2019**, *9*, 20295.
[25] L. Nedelchev, D. Ivanov, N. Berberova, V. Strijkova, D. Nazarova, *Opt. Quantum Electron.* **2018**, *50*, 212.
[26] K. J. Park, J. H. Park, J.-H. Huh, C. H. Kim, D. H. Ho, G. H. Choi, P. J. Yoo, S. M. Cho, J. H. Cho, S. Lee, *ACS Appl. Mater. Interfaces* **2017**, *9*, 9935.
[27] S. Nair, C. Escobedo, R. G. Sabat, *ACS Sens.* **2017**, *2*, 379.
[28] C. Probst, C. Meichner, K. Kreger, L. Kador, C. Neuber, H.-W. Schmidt, *Adv. Mater.* **2016**, *28*, 2624.
[29] S. Loebner, J. Jelken, N. Yadavalli, E. Sava, N. Hurduc, S. Santer, *Molecules* **2016**, *21*, 1663.
[30] J. Choi, W. Cho, Y. S. Jung, H. S. Kang, H.-T. Kim, *ACS Nano* **2017**, *11*, 1320.
[31] F. Martino, A. R. Perestrelo, V. Vinarský, S. Pagliari, G. Forte, *Front. Physiol.* **2018**, *5*, 824.
[32] D. E. Ingber, *FASEB J.* **2006**, *20*, 811.
[33] V. Y. Chang, C. Fedele, A. Priimagi, A. Shishido, C. J. Barrett, *Adv. Opt. Mater.* **2019**, *7*, 1900091.
[34] M. Salvatore, S. L. Oscurato, M. D'Albore, V. Guarino, S. Zeppetelli, P. Maddalena, A. Ambrosio, L. Ambrosio, *J. Funct. Biomater.* **2020**, *11*, 8.
[35] L. Rocha, C. M. Păiuş, A. Luca-Raicu, E. Resmerita, A. Rusu, I. A. Moleavin, M. Hamel, N. Branza-Nichita, N. Hurduc, *J. Photochem. Photobiol., A* **2014**, *291*, 16.
[36] J. K. Kular, S. Basu, R. I. Sharma, *J. Tissue Eng.* **2014**, *5*, 2041731414557112.
[37] C. Frantz, K. M. Stewart, V. M. Weaver, *J. Cell Sci.* **2010**, *123*, 4195.
[38] B. M. Baker, B. Trappmann, W. Y. Wang, M. S. Sakar, I. L. Kim, V. B. Shenoy, J. A. Burdick, C. S. Chen, *Nat. Mater.* **2015**, *14*, 1262.
[39] T. R. Cox, J. T. Erler, *Dis. Models Mech.* **2011**, *4*, 165.
[40] C. Fedele, E. Mäntylä, B. Belardi, T. Hamkins-Indik, S. Cavalli, P. A. Netti, D. A. Fletcher, S. Nymark, A. Priimagi, T. O. Ihalainen, *Sci. Rep.* **2020**, *10*, 15329.
[41] C. Rianna, A. Calabuig, M. Ventre, S. Cavalli, V. Pagliarulo, S. Grilli, P. Ferraro, P. A. Netti, *ACS Appl. Mater. Interfaces* **2015**, *7*, 16984.
[42] G. Koçer, J. ter Schiphorst, M. Hendrikx, H. G. Kassa, P. Leclère, A. P. H. J. Schenning, P. Jonkheijm, *Adv. Mater.* **2017**, *29*, 1606407.
[43] M. Ristola, C. Fedele, S. Hagman, L. Sukki, F. E. Kapucu, R. Mzezewa, T. Hyvärinen, P. Kallio, A. Priimagi, S. Narkilahti, *Adv. Mater. Interfaces* **2021**, *8*, 2100048.
[44] H. Baac, J.-H. Lee, J.-M. Seo, T. H. Park, H. Chung, S.-D. Lee, S. J. Kim, *Mater. Sci. Eng. C* **2004**, *24*, 209.
[45] S. De Martino, S. Cavalli, P. A. Netti, *Adv. Healthcare Mater.* **2020**, *9*, 2000470.
[46] S. Bian, J. M. Williams, D. Y. Kim, L. Li, S. Balasubramanian, J. Kumar, S. Tripathy, *J. Appl. Phys.* **1999**, *86*, 4498.
[47] A. Tofini, L. Levesque, O. Lebel, R. G. Sabat, *J. Mater. Chem. C* **2018**, *6*, 1083.
[48] J. Vapaavuori, R. H. A. Ras, M. Kaivola, C. G. Bazuin, A. Priimagi, *J. Mater. Chem. C* **2015**, *3*, 11011.
[49] T. Ubukata, T. Isoshima, M. Hara, *Adv. Mater.* **2005**, *17*, 1630.
[50] J. Krüger, N. Bolle, T. Calvelo, S. Bergmann, H. Abourahma, D. J. McGee, *J. Appl. Phys.* **2019**, *125*, 243108.
[51] S. De Martino, P. A. Netti, *Biophys. Rev.* **2020**, *1*, 011302.
[52] M. Hendrikx, J. ter Schiphorst, E. P. A. van Heeswijk, G. Koçer, C. Knie, D. Bléger, S. Hecht, P. Jonkheijm, D. J. Broer, A. P. H. J. Schenning, *Small* **2018**, *14*, 1803274.
[53] J. Kim, R. C. Hayward, *Trends Biotechnol.* **2012**, *30*, 426.
[54] R. P. Berkelaar, P. Bampoulis, E. Dietrich, H. P. Jansen, X. Zhang, E. S. Kooij, D. Lohse, H. J. W. Zandvliet, *Langmuir* **2015**, *31*, 1017.
[55] R. Kirby, R. G. Sabat, J. M. Nunzi, O. Lebel, *J. Mater. Chem. C* **2014**, *2*, 841.
[56] D. Li, X. Zhao, *Colloids Surf., A* **2014**, *459*, 128.
[57] A. Natansohn, P. Rochon, *Chem. Rev.* **2002**, *102*, 4139.
[58] M. Dumont, A. El Osman, *Chem. Phys.* **1999**, *245*, 437.
[59] S. L. Oscurato, M. Salvatore, P. Maddalena, A. Ambrosio, *Nanophotonics* **2018**, *7*, 1387.
[60] M. Saphiannikova, V. Toshchevikov, *J. Soc. Inf. Disp.* **2015**, *23*, 146.
[61] H. Huang, Z. Wang, X. Li, F. Yang, Y. Su, J. Xu, X. Wang, *RSC Adv.* **2021**, *11*, 15387.
[62] F. Pirani, A. Angelini, F. Frascella, R. Rizzo, S. Ricciardi, E. Descrovi, *Sci. Rep.* **2016**, *6*, 31702.
[63] Y. Wang, H. Wang, S. Bi, B. Guo, *Beilstein J. Nanotechnol.* **2015**, *6*, 952.

[64] D. Li, D. Jing, Y. Pan, W. Wang, X. Zhao, *Langmuir* **2014**, *30*, 6079.
[65] A. Agrawal, J. Park, D. Y. Ryu, P. T. Hammond, T. P. Russell, G. H. McKinley, *Nano Lett.* **2005**, *5*, 1751.
[66] Y. Wang, B. Bhushan, X. Zhao, *Nanotechnology* **2009**, *20*, 045301.
[67] Z. Zhang, Z. Wang, R. Xing, Y. Han, *Surf. Sci.* **2003**, *539*, 129.
[68] E. Bonaccurso, H. J. Butt, V. Franz, K. Graf, M. Kappl, S. Loi, B. Niesenhaus, S. Chemnitz, M. Böhm, B. Petrova, U. Jonas, H. W. Spiess, *Langmuir* **2002**, *18*, 8056.
[69] L. Xu, T. Shi, L. An, *Langmuir* **2007**, *23*, 9282.
[70] C. Luo, R. Xing, Z. Zhang, J. Fu, Y. Han, *J. Colloid Interface Sci.* **2004**, *269*, 158.
[71] L. Xue, Y. Han, *Prog. Polym. Sci.* **2011**, *36*, 269.
[72] K. Ahmad, X. Zhao, Y. Pan, D. Hussain, *Beilstein J. Nanotechnol.* **2016**, *7*, 581.
[73] E. A. Jagla, *Phys. Rev. B: Condens. Matter Mater. Phys.* **2007**, 75.
[74] M. Maebayashi, T. Matsuoka, S. Koda, R. Hashitani, T. Nishio, S. I. Kimura, *Polymer* **2004**, *45*, 7563.
[75] B. Jing, J. Zhao, Y. Wang, X. Yi, H. Duan, *Langmuir* **2010**, *26*, 7651.
[76] C. A. Featherston, *Int. J. Non-Linear Mech.* **2000**, *35*, 515.
[77] M. H. Nazir, Z. A. Khan, *Eng. Failure Anal.* **2017**, *72*, 80.
[78] T. J. Giammaria, F. Ferrarese Lupi, G. Seguini, K. Sparnacci, D. Antonioli, V. Gianotti, M. Laus, M. Perego, *ACS Appl. Mater. Interfaces* **2017**, *9*, 31215.
[79] K. Sparnacci, R. Chiarcos, V. Gianotti, M. Laus, T. J. Giammaria, M. Perego, G. Munaò, G. Milano, A. De Nicola, M. Haese, L. P. Kreuzer, T. Widmann, P. Müller-Buschbaum, *ACS Appl. Mater. Interfaces* **2020**, *12*, 7777.
[80] J. García-Turiel, B. Jérôme, *Colloid Polym. Sci.* **2007**, *285*, 1617.
[81] J. Perlich, V. Körstgens, E. Metwalli, L. Schulz, R. Georgii, P. Müller-Buschbaum, *Macromolecules* **2009**, *42*, 337.
[82] A. A. Griffith, *Philos. Trans. Royal Soc. A* **1921**, *221*, 163.
[83] S. Loebner, N. Lomadze, A. Kopyshev, M. Koch, O. Guskova, M. Saphiannikova, S. Santer, *J. Phys. Chem. B* **2018**, *122*, 2001.
[84] Y. Li, Y. He, X. Tong, X. Wang, *J. Am. Chem. Soc.* **2005**, *127*, 2402.
[85] J. Wang, S. Wang, Y. Zhou, X. Wang, Y. He, *ACS Appl. Mater. Interfaces* **2015**, *7*, 16889.
[86] H. Huang, Y. Su, J. Xu, X. Wang, *Langmuir* **2019**, *35*, 15295.
[87] S. Lee, H. S. Kang, A. Ambrosio, J. K. Park, L. Marrucci, *ACS Appl. Mater. Interfaces* **2015**, *7*, 8209.
[88] H. Huang, Y. Su, X. Zhou, C. Liao, C. Hsu, Y. Du, J. Xu, X. Wang, *Soft Matter* **2018**, *14*, 5847.
[89] S. Lee, H. S. Kang, A. Ambrosio, J.-K. Park, L. Marrucci, *ACS Appl. Mater. Interfaces* **2015**, *7*, 8209.
[90] N. Li, G. Ye, Y. He, X. Wang, *Chem. Commun.* **2011**, *47*, 4757.
[91] A. Ambrosio, S. Girardo, A. Camposeo, D. Pisignano, P. Maddalena, *Appl. Phys. Lett.* **2013**, *102*, 093102.
[92] C. Hubert, C. Fiorini-Debuisschert, I. Maurin, J.-M. Nunzi, P. Raimond, *Adv. Mater.* **2002**, *14*, 729.
[93] H. Leblond, R. Barille, S. Ahmadi-Kandjani, J. M. Nunzi, E. Ortyl, S. Kucharski, *J. Phys. B: At., Mol. Opt. Phys.* **2009**, *42*, 205401.
[94] X. Wang, J. Yin, X. Wang, *Langmuir* **2011**, *27*, 12666.
[95] H. Galinski, A. Ambrosio, P. Maddalena, I. Schenker, R. Spolenak, F. Capasso, *Proc. Natl. Acad. Sci. U. S. A.* **2014**, *111*, 17017.
[96] J. Noga, A. Sobolewska, S. Bartkiewicz, M. Virkki, A. Priimagi, *Macromol. Mater. Eng.* **2017**, *302*, 1600329.
[97] C. Brown, S. K. Rastogi, S. L. Barrett, H. E. Anderson, E. Twichell, S. Gralinski, A. McDonald, W. J. Brittain, *J. Photochem. Photobiol., A* **2017**, *336*, 140.
[98] M. Kameda, K. Sumaru, T. Kanamori, T. Shinbo, *J. Appl. Polym. Sci.* **2003**, *88*, 2068.
[99] M. Gillono, I. Roppolo, F. Frascella, L. Scaltrito, C. F. Pirri, A. Chiappone, *Appl. Mater. Today* **2020**, *18*, 100470.
[100] W.-P. Huang, X.-C. Chen, M. Hu, J. Wang, H.-L. Qian, D.-F. Hu, R.-L. Dong, S.-Y. Xu, K.-F. Ren, J. Ji, *ACS Appl. Mater. Interfaces* **2020**, *12*, 42081.
[101] M. K. Purkait, M. K. Sinha, P. Mondal, R. Singh, in *Stimuli Responsive Polymeric Membranes* (Eds: M. K. Purkait, M. K. Sinha, P. Mondal, R. Singh), Elsevier, Amsterdam **2018**, pp. 115–144.
[102] E. Berthier, E. W. K. Young, D. Beebe, *Lab Chip* **2012**, *12*, 1224.
[103] M. Isomäki, C. Fedele, L. Kääriäinen, E. Mäntylä, S. Nymark, T. O. Ihalainen, A. Primaagi, *Small Sci.* **2022**, 2100099, https://doi.org/10.1002/smsc.202100099.
[104] B. Audia, P. Pagliusi, C. Provenzano, A. Roche, L. Oriol, G. Cipparrone, *ACS Appl. Polym. Mater.* **2020**, *2*, 1597.
[105] H. Rekola, A. Berdin, C. Fedele, M. Virkki, A. Priimagi, *Sci. Rep.* **2020**, *10*, 19642.
[106] I. Horcas, R. Fernández, J. M. Gómez-Rodríguez, J. Colchero, J. Gómez-Herrero, A. M. Baro, *Rev. Sci. Instrum.* **2007**, *78*, 013705.
[107] C. A. Schneider, W. S. Rasband, K. W. Eliceiri, *Nat. Methods* **2012**, *9*, 671.